Available online at www.sciencedirect.com
ScienceDirect
Robotics and Computer-Integrated Manufacturing 24 (2008) 60–76
Robotics and Computer-Integrated Manufacturing
www.elsevier.com/locate/rcim

On the workspace boundary determination of serial manipulators with non-unilateral constraints

Jingzhou Yang[a,*], Karim Abdel-Malek[a], Yunqing Zhang[b]

[a]*Virtual Soldier Research (VSR) Program, Center for Computer-Aided Design, The University of Iowa, 111 Engineering Research Facility, Iowa City, IA 52242-1000, USA*

[b]*National Engineering Research Center for CAD, Huazhong University of Science & Technology, Wuhan, Hubei, 430074, PR China*

Received 2 July 2005; received in revised form 13 March 2006; accepted 26 June 2006

Abstract

Broadly applicable analytical algorithms for workspace of serial manipulators with non-unilateral constraints are developed and illustrated. The Jacobian row-rank deficiency method is employed to determine the singularities of these manipulators. There are four types of singularity sets: Type I: position Jacobian singularities; Type II: instantaneous singularities that are due to a generalized joint that is reaching its apex; Type III: domain boundary singularities, which are associated with the initial and final values of the time interval; Type IV: coupled singularities, which are associated with a relative singular Jacobian, where the null space is reduced in one sub-matrix due to either of two occurrences: a Type II or a Type III singularity. All of the singular surfaces are hypersurfaces that extend internally and externally the workspace envelope. Intersecting singular surfaces identifies singular curves that partition singular surfaces into subsurfaces, and a perturbation method is used to identify regions (curve segments/surface patches) of the hypersurfaces that are on the boundary. The formulation is illustrated by implementing it to a spatial 3-degree of freedom (DOF) and a spatial 4-DOF manipulator.

Keywords: Non-unilateral; Jacobian row-rank deficiency; Hypersurfaces; Workspace envelope; Perturbation method

1. Introduction

Considerable effort has been directed towards formulations of mathematical methods for determining workspaces of manipulators. The study of manipulator workspaces has been identified in the fields of manufacturing for efficient placement of robots on the shop floor and for securing the maximum functionality of a manipulator in terms of dexterity. Other applications environments include the medical field, where the use of mechanisms and machines in medical interventions has become very common, and in the manufacturing arena, where manipulators are used for welding, painting, etc.

Vinagradov [36], in one of the earliest studies on the subject of manipulator performance in terms of workspace, introduced the term ''service sphere''. Roth [29] introduced the relationship between kinematic geometry and manipulator performance, including workspace. A numerical approach to this relationship, by tracing boundary surfaces of a workspace was formulated and solved by Kumar and Waldron [21]. The reciprocal screw method [34] for workspace generation is based on the fact that when the end-effector reference point of the manipulator is on the workspace boundary; all joint axes of a manipulator are reciprocal to a zero pitch wrench axis. For each degree-of-freedom (DOF) lost, there exists one reciprocal screw which, if applied as a wrench to the end-effector, produces no virtual work for the

*Corresponding author. Tel.: +1319 353 2249; fax: +1319 384 0542.
E-mail address: jyang@engineering.uiowa.edu (J. Yang).
URL: http://www.digital-humans.org.

0736-5845/$ - see front matter © 2006 Elsevier Ltd. All rights reserved.
doi:10.1016/j.rcim.2006.06.005

manipulator joints. Wang and Waldron [38], based upon earlier work [37], stated that the Jacobian of the manipulator becomes singular if its columns, which are screw quantities, do not span the full rank of the matrix, thus reducing the Jacobian rank by at least one.

Litvin [23] used the implicit function theorem to define singular configurations of mechanisms as criteria for boundaries of workspaces. An enumeration of singular configurations due to the vanishing of the determinant of the Jacobian and the Jacobian's minors was presented by Lipkin and Pohl [22]. Shamir [30] provided an analytical tool to determine whether the singularities are avoidable for 3-DOF manipulators. Analytical conditions associated with special features of the geometry of specific manipulators have been used by a several researchers to obtain explicit criteria for boundaries of workspaces [15,31,35,42]. Singularity of the velocity transformation between input and output coordinates has been used to characterize singular surfaces of manipulators [21,37]. Other studies on the subject of manipulator workspaces can be found in Gupta [18], Sugimoto and Duffy [33], Davidson and Hunt [11], Agrawal [4], Gosselin and Angeles [17], Emiris [14], Pennock and Kassner [27], Ceccarelli [9], and Zhang et al. [41].

Haug et al. [20] formulated numerical criteria for finding the accessible output set of a general multi-DOF system using a continuation method to trace boundary curves suitable for the study of both open- and closed-loop manipulators. The initial criteria for this computational method were presented by Haug et al. [19] and Wang and Wu [39]. The algorithm computes tangent vectors at bifurcation points of continuation curves that define the boundary of manipulator workspaces. A cross-section of the workspace is obtained, and boundary continuation curves are traced. Qiu et al. [28] demonstrated this method for a closed-loop mechanism called the Stewart Platform, where continuation curves are evaluated on the exterior boundary of the accessible output set. These curves are then assembled into a mesh that is enveloped by appropriate surface patches. This method has proven valid for determining the general shape of the accessible output set. Its main difficulty is in determining the status of the singularity points along continuation curves. Although singular behavior occurring at points along the curves is identified, this method is completely numerical and only traces boundary curves. It does not result in analytical surfaces bounding the accessible output set. An algebraic formulation for determining the workspace of four-revolute manipulators was recently presented by Ceccarelli and Vinciguerra [8]. This method can determine holes and voids in the accessible output set. Bulca et al. [6] developed a technique, based on the Euler–Rodrigues parameters of the rotation of a rigid body, for determining the workspace of spherical platform mechanisms. Cavusoqlu et al. [7] proposed a quantitative method to evaluate the kinematic ability of surgical manipulators to perform the critical tasks of suturing and knot-tying. Their proposed method does not require a physical prototype; instead, it runs typical tool motions during these tasks through the inverse kinematics of the manipulators and checks the system for its ability to accommodate the desired motions. Wang et al. [40] introduced the workspace analysis of a special manipulator, which is a closed-chain design offering high payload, high stiffness, and low inertia, but at the expense of limited workspace. The resulting workspace is shown to be complex, but manageable, which enables it to be used for on-line planning and collision avoidance. Snyman et al. [45] presented an optimization-based approach for determining the boundaries of serial and parallel manipulator workspaces. Monsarrat and Gosselin [24] introduced the determination of the singularity loci of a 6-DOF spatial parallel platform mechanism of a new type that can be statically balanced. St-Onge and Gosselin [32] studied the singularity loci of the Gough–Stewart platform and obtain a graphical representation of these loci in the manipulator's workspace. Ceccarelli and Ottaviano [10] proposed a numerical procedure for determining and evaluating the workspace of the eclipse robot architecture, which is a novel parallel architecture. Di Gregorio and Zanforlin [13] reported the analytic expression of the surfaces bounding the workspace in the coordinates of a platform point, which contains all the manipulator geometric parameters by a fourth degree polynomial equation. This analytic expression is given in an explicit form.

In our earlier work [1–3], we used singular behavior to identify the serial manipulator, where only unilateral constraints were considered. Yang and Abdel-Malek [43] extended the Jacobian row-rank deficiency method to serial manipulators with non-unilateral constraints and studied the singular behavior. Yang and Abdel-Malek [44] studied the singular characteristics for both unilateral and un-unilateral constraints. In this paper, we first apply Jacobian row-rank deficiency conditions to determine the singular hypersurfaces of manipulators with non-unilateral constraints, then implement surface/surface intersection to partition singular surfaces, finally, propose a perturbation algorithm to identify the boundary of the workspace, where joints are described as functions of time and where each joint may or may not be independent of another joint.

2. Formulation

In order to find the analytical boundary of the manipulator workspace, the kinematics of the underlying mechanism will be formulated. In this section, we will (1) define the unilateral and non-unilateral constraints, (2) determine singular surfaces, (3) determine singular curves that partition singular surfaces to subsurfaces and identify which subsurfaces are on the boundary.

2.1. Unilateral and non-unilateral constraints

We define $\mathbf{q} \in \Re^n$ as the vector of n-generalized joint coordinates characterizing a manipulator configuration. The vector function generated by a point on the end-effector of a serial arm, written as a multiplication of rotation matrices and position vectors, is expressed by

$$\mathbf{\Phi}(\mathbf{q}(\mathbf{t})) = \begin{bmatrix} x(\mathbf{q}(\mathbf{t})) \\ y(\mathbf{q}(\mathbf{t})) \\ z(\mathbf{q}(\mathbf{t})) \end{bmatrix} = \sum_{i=1}^{i=n} \left[\prod_{j=1}^{j=i-1} {}^{j-1}\mathbf{R}_j \right] {}^{i-1}\mathbf{p}_i, \tag{1}$$

where $\mathbf{q}(\mathbf{t}) = [\, q_1(t_1) \quad q_2(t_2) \quad \cdots \quad q_n(t_n)\,]^{\mathrm{T}}$, $\mathbf{t} = [\, t_1 \quad \cdots \quad t_n\,]^{\mathrm{T}}$ is the vector of time variables for each joint, and both ${}^{i}\mathbf{p}_j$ and ${}^{i}\mathbf{R}_j$ are defined using the Denavit–Hartenberg representation method [12,16] such that

$${}^{i-1}\mathbf{R}_i = \begin{bmatrix} \cos\theta_i & -\cos\alpha_i \sin\theta_i & \sin\alpha_i \sin\theta_i \\ \sin\theta_i & \cos\alpha_i \cos\theta_i & -\sin\alpha_i \cos\theta_i \\ 0 & \sin\alpha_i & \cos\alpha_i \end{bmatrix} \tag{2}$$

and

$${}^{(i-1)}\mathbf{p}_i = [\, a_i \cos\theta_i \quad a_i \quad \sin\theta_i \quad d_i\,]^{\mathrm{T}}, \tag{3}$$

where θ_i is the joint angle from $\mathbf{x}_{i-1}$ axis to the $\mathbf{x}_i$ axis, d_i is the shortest distance between $\mathbf{x}_{i-1}$ and $\mathbf{x}_i$ axes, a_i is the offset distance between $\mathbf{z}_i$ and $\mathbf{z}_{i-1}$ axes, and α_i is the offset angle from $\mathbf{z}_{i-1}$ and $\mathbf{z}_i$ axes. The generalized variable is $q_i = d_i$ if the joint is prismatic, and $q_i = \theta_i$ if the joint is revolute.

The joint angle q_i is defined by $q_i = f(t_i)$ and $t_i^{\mathrm{L}} \leqslant t_i \leqslant t_i^{\mathrm{U}}$, where L denotes the lower limit, and U denotes the upper limit. If $f(t_i)$ is a monotonic increasing function and there also exists $\mathrm{d}f(t_i)/\mathrm{d}t_i \neq 0$ for $t_i \in (t_i^{\mathrm{L}}, t_i^{\mathrm{U}})$, then q_i is called unilateral constraints (e.g. Fig. 1(a)). For any joint function $q_j = g(t_j)$ and $t_j^{\mathrm{L}} \leqslant t_j \leqslant t_j^{\mathrm{U}}$, if there exists $\mathrm{d}g(t_j)/\mathrm{d}t_j = 0$ for $t_j \in (t_j^{\mathrm{L}}, t_j^{\mathrm{U}})$, then q_j is called non-unilateral constraints (e.g. Fig. 1(b)), where $i,j = 1,\ldots,n$.

Although the user give the joint limits $q_i^{\mathrm{L}} \leqslant q_i \leqslant q_i^{\mathrm{U}}$, the real joint profiles are unilateral or non-unilateral constraints. It is obvious that the singularities of manipulators are different for unilateral and non-unilateral cases. This paper focuses on the workspace boundary determination of manipulators with non-unilateral constraints.

2.2. Singularity analysis

The vector function $\mathbf{\Phi}(\mathbf{q}(\mathbf{t}))$ in Eq. (1) characterizes the set of all points inside and on the boundary of the workspace as a function of time for non-unilateral constraints. The aim of this work is to determine the boundary to this set and to analytically represent it.

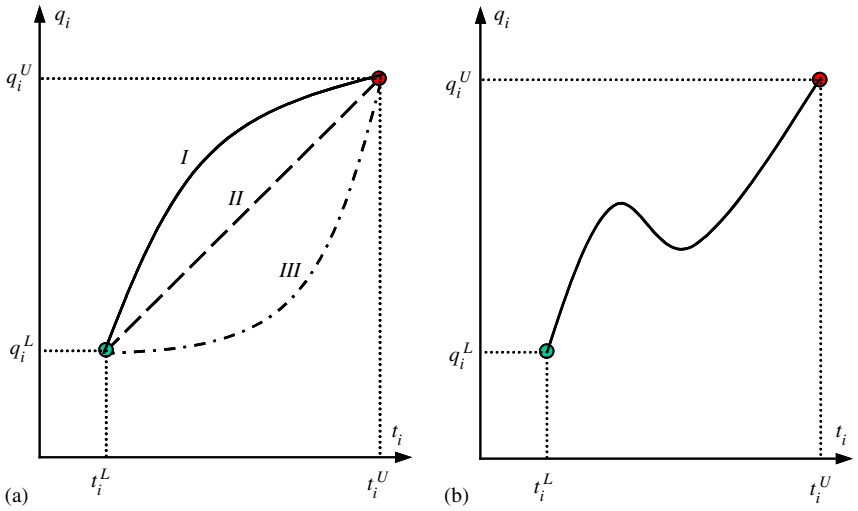

Fig. 1. Joint profiles: (a) Unilateral constraints; (b) Non-unilateral constraints.

At a specified position in space $\mathbf{x} = [x^0 \quad y^0 \quad z^0]^T$, Eq. (1) can be written as a constraint function

$$\mathbf{\Omega}(\mathbf{q}(\mathbf{t})) = \begin{bmatrix} x(\mathbf{q}(\mathbf{t})) - x^0 \\ y(\mathbf{q}(\mathbf{t})) - y^0 \\ z(\mathbf{q}(\mathbf{t})) - z^0 \end{bmatrix} = \mathbf{0} \tag{4}$$

and the joint functions can be written as a constraint function

$$\mathbf{\Gamma}(\mathbf{t}) = \begin{bmatrix} q_1(t_1) - q_1(t_1^0) \\ \vdots \\ q_n(t_n) - q_n(t_n^0) \end{bmatrix} = \mathbf{0}, \tag{5}$$

where constraints on the time variables are imposed in terms of inequalities in the form of $t_i^L \leqslant t_i \leqslant t_i^U$, where $i = 1, \ldots n$, are transformed into a parametric equation by introducing a new set of generalized coordinates $\lambda = [\lambda_1, \lambda_2, \ldots, \lambda_n]^T$ such that

$$t_i = ((t_i^L + t_i^U)/2) + ((t_i^U - t_i^L)/2) \sin \lambda_i \quad i = 1, \ldots, n. \tag{6}$$

Eq. (6) can be written as $\mathbf{t} = \mathbf{\Pi}(\boldsymbol{\lambda})$. In the field of optimization, these generalized coordinates λ_i are called *slack variables*. They effectively enable inequality constraints to be considered into the formulation. In order to include the effect of joints with non-unilateral constraints and time limits, augmentation of the constraint equation $\mathbf{\Omega}(\mathbf{q}(\mathbf{t}))$ with the parameterized inequality constraints is proposed, such that

$$\mathbf{H}(\mathbf{q}^*) = \begin{bmatrix} x(\mathbf{q}(\mathbf{t})) - x^0 \\ y(\mathbf{q}(\mathbf{t})) - y^0 \\ z(\mathbf{q}(\mathbf{t})) - z^0 \\ q_i(t_i) - q_i(t_i^0) \\ t_i - ((t_i^L + t_i^U)/2) - ((t_i^U - t_i^L)/2) \sin \lambda_i \end{bmatrix} = \mathbf{0} \quad i = 1, \ldots n, \tag{7}$$

where $\mathbf{q}^* = [\mathbf{q}^T \quad \mathbf{t}^T \quad \lambda^T]^T$ is the vector of all generalized coordinates. Note that although $2n$ new variables (t_i and λ_i) have been added, $2n$ equations have also been added to the constraint vector function, without losing the dimensionality of the problem.

To implement the Implicit Function Theorem, we investigate the *Jacobian* of the constraint function $\mathbf{H}(\mathbf{q}^*)$ at a point $\mathbf{q}^{*0}$ is the $(3+2n) \times 3n$ matrix

$$\mathbf{H}_{\mathbf{q}^*}(\mathbf{q}^{*0}) = \partial \mathbf{H} / \partial \mathbf{q}^*, \tag{8}$$

where the subscript denotes a derivative. With the modified formulation including the parameterized inequality constraints, the Jacobian is expanded as

$$\mathbf{H}_{\mathbf{q}^*} = \begin{bmatrix} \mathbf{\Phi}_\mathbf{q} & \mathbf{0}_1 & \mathbf{0}_2 \\ \mathbf{I} & \mathbf{\Gamma}_\mathbf{t} & \mathbf{0}_3 \\ \mathbf{0}_4 & \mathbf{I} & \mathbf{t}_{\boldsymbol{\lambda}} \end{bmatrix}, \tag{9}$$

where the notation x_{q1} denotes the partial derivative of x with respect to q_1, i.e., $\partial x / \partial q_1$, and

$$\mathbf{\Phi}_\mathbf{q} = \begin{bmatrix} x_{q_1} & x_{q_2} & \cdots & x_{q_n} \\ y_{q_1} & y_{q_2} & \cdots & y_{q_n} \\ z_{q_1} & z_{q_2} & \cdots & z_{q_n} \end{bmatrix}, \quad \mathbf{\Gamma}_\mathbf{t} = \dot{\mathbf{q}} = \begin{bmatrix} \dfrac{dq_1}{dt_1} & 0 & \cdots & 0 \\ 0 & \dfrac{dq_2}{dt_2} & \cdots & 0 \\ \vdots & \vdots & \ddots & \vdots \\ 0 & 0 & \cdots & \dfrac{dq_n}{dt_n} \end{bmatrix}$$

and

$$\mathbf{t}_\lambda = \begin{bmatrix} -((t_1^{\mathrm{U}} - t_1^{\mathrm{L}})/2)\cos\lambda_1 & 0 & \cdots & 0 \\ 0 & -((t_2^{\mathrm{U}} - t_2^{\mathrm{L}})/2)\cos\lambda_2 & \cdots & 0 \\ \cdots & \cdots & \ddots & \cdots \\ 0 & 0 & 0 & -((t_n^{\mathrm{U}} - t_n^{\mathrm{L}})/2)\cos\lambda_n \end{bmatrix}$$

are diagonal block matrices, $\mathbf{0}_1$ and $\mathbf{0}_2$ are $(3\times n)$ zero matrices, $\mathbf{0}_3$ and $\mathbf{0}_4$ are $(n\times n)$ zero matrices, and $\mathbf{I}$ is $(n\times n)$ an identity matrix.

We define the *boundary of the workspace* ∂W (workspace envelope) as a subset of the *workspace* at which the Jacobian of the constraint function of Eq. (7) is row-rank deficient, i.e.,

$$\partial W \subset \{\text{Rank } \mathbf{H}_{\mathbf{q}^*}(\mathbf{q}^*) < k, \text{ for some } \mathbf{q}^* \text{ with } \mathbf{H}(\mathbf{q}^*) = \mathbf{0}\} \tag{10}$$

where k is at least $(3+2n-1)$. For an n-DOF system, the Jacobian $\mathbf{H}_{\mathbf{q}^*}(\mathbf{q}^{*0})$ is row-rank deficient if and only if one of the following conditions are satisfied.

2.2.1. Type I: Jacobian singularities

If there are no t_i that reach their limits, i.e., $t_i \neq t_i^{\mathrm{U}}$ and $t_i \neq t_i^{\mathrm{L}}$, and there are no joints with $\mathrm{d}q_i/\mathrm{d}t_i = 0$, the diagonal submatrices $[\mathbf{\Gamma_t}]$ and $[\mathbf{t_\lambda}]$ are full row rank. Therefore, the only possibility for $[\mathbf{H}_{\mathbf{q}^*}]$ to be row-rank deficient is when the block matrix $[\mathbf{\Phi_q}]$ is row-rank deficient. Define two independent sub-vectors of $\mathbf{q}$ as $\mathbf{p}$ and $\mathbf{u}$, where

$$\mathbf{q} = [\,\mathbf{p}^{\mathrm{T}} \quad \mathbf{u}^{\mathrm{T}}\,]^{\mathrm{T}} \quad \text{where } \mathbf{p}, \mathbf{u} \in \mathbf{q} \text{ and } \mathbf{p} \cap \mathbf{u} = \phi. \tag{11}$$

If $\mathbf{u} \in \mathbf{R}^m$ then $\mathbf{p} \in \mathbf{R}^{(n-m)}$.

Type I singularity set can be defined as

$$S^{(1)} \equiv \{\mathbf{p} \in \mathbf{q} : \text{Rank}[\mathbf{\Phi_q}] < 3 \quad \text{for some constant subset of } \mathbf{q}\}, \tag{12}$$

where $\mathbf{p}$ is within the specified joint limit constraints.

2.2.2. Type II: instantaneous singularities

When we find there are m $(m \geqslant 2)$ joints that have $\mathrm{d}q_i/\mathrm{d}t_i = 0$, then Type II singularities are

$$S^{(2)} \equiv \{\mathbf{p} \in \Re^{(n-2)} : \mathbf{p} \equiv \partial\mathbf{t}^{\mathrm{inst}} = [t_i^{\mathrm{inst}}, t_j^{\mathrm{inst}}, \ldots]\}. \tag{13}$$

2.2.3. Type III singularities

Type III singularities are defined as

$$S^{(3)} \equiv \{\mathbf{p} \in \Re^{(n-2)} : \mathbf{p} \equiv \partial\mathbf{t}^{\mathrm{inst}} \cup \partial\mathbf{t}^{\mathrm{Limit}} = [t_i^{\mathrm{inst}}, t_j^{\mathrm{inst}}, \ldots] \cup [t_i^{\mathrm{limit}}, t_j^{\mathrm{limit}}, \ldots]\}. \tag{14}$$

2.2.4. Type IV: coupled singularities

When certain t_i reach their limits, e.g., $[t_i, t_j, t_k] = [t_i^{\mathrm{limit}}, t_j^{\mathrm{limit}}, t_k^{\mathrm{limit}}]$, the corresponding diagonal elements in the matrix $[\mathbf{t_\lambda}]$ will be equal to zero. For example, if $t_i = t_i^{\mathrm{L}}$ (or t_i^{U}), the diagonal element of $[\partial\mathbf{t}/\partial\lambda]_{ii}$ will be zero (i.e., $b_i\cos\lambda_i$ is zero for either $i = 1, \ldots, n$ where t_i has reached a limit). When certain t_i reach their instantaneous points (e.g., $\mathrm{d}q_i/\mathrm{d}t_i = 0$), e.g., $[t_i, t_j, t_k] = [t_i^{\mathrm{inst}}, t_j^{\mathrm{inst}}, t_k^{\mathrm{inst}}]$, the corresponding diagonal elements in the matrix $[\mathbf{\Gamma_t}]$ will be equal to zero.

Solving the row-rank deficiency condition for Eq. (7) is equivalent to solving the rank deficiency for

$$[\mathbf{\Phi_q} \not\subset [\mathbf{\Phi}_{q_i}, \mathbf{\Phi}_{q_j}, \mathbf{\Phi}_{q_k}]] \tag{15}$$

with

$$q_i = q_i^{\mathrm{limit}}, q_j = q_j^{\mathrm{limit}}, q_k = q_k^{\mathrm{limit}} \text{ or } q_i = q_i^{\mathrm{inst}}, q_j = q_j^{\mathrm{inst}},$$
$$q_k = q_k^{\mathrm{inst}},$$

where the notation of Eq. (15) represents the exclusion of the right matrix from the left matrix, and it represents the submatrix of $[\mathbf{\Phi_q}]$ when t_i are at their limits or instantaneous points.

From the foregoing observation, the fourth type of singular sets is formulated. Define a new vector $\partial\mathbf{q}(\mathbf{t}^{\mathrm{limit}}) = [q_i(t^{\mathrm{limit}}), q_j(t^{\mathrm{limit}}), q_k(t^{\mathrm{limit}})]^{\mathrm{T}}$, or $\partial\mathbf{q}(\mathbf{t}^{\mathrm{inst}}) = [q_i(t^{\mathrm{inst}}), q_j(t^{\mathrm{inst}}), q_k(t^{\mathrm{inst}})]^{\mathrm{T}}$, which is a sub-vector of $\mathbf{q}$ where

$$1 \leqslant \dim(\partial\mathbf{q}(\mathbf{t}^{\mathrm{limit}} \text{ or } \mathbf{t}^{\mathrm{inst}})) \leqslant (n-3). \tag{16}$$

For the case of $\dim(\partial\mathbf{q}(\mathbf{t}^{\text{limit}} \text{ or } \mathbf{t}^{\text{inst}})) = (n-2)$, note that the solution of Eq. (7) is readily available, as will be discussed in the following sections. The joint coordinates can be partitioned as

$$\mathbf{q} = [\mathbf{w}^{\mathrm{T}}, \partial\mathbf{q}(\mathbf{t}^{\text{limit}} \text{ or } \mathbf{t}^{\text{inst}})^{\mathrm{T}}]^{\mathrm{T}} \quad \text{and} \quad \mathbf{w} \cap \partial\mathbf{q}(\mathbf{t}^{\text{limit}} \text{ or } \mathbf{t}^{\text{inst}}) = \phi. \tag{17}$$

Then, if $[\boldsymbol{\Phi}_{\mathbf{w}}(\mathbf{w}, \partial\mathbf{q}(\mathbf{t}^{\text{limit}} \text{ or } \mathbf{t}^{\text{inst}}))]$ is row-rank deficient, the subJacobian $[\boldsymbol{\Phi}_{\mathbf{q}}]$ is also rank deficient. Let the solution for this condition be denoted by $\hat{\mathbf{p}}$, which is a constant subvector of $\mathbf{w}$, and $\mathbf{w} = [\mathbf{u}^{\mathrm{T}}, \hat{\mathbf{p}}^{\mathrm{T}}]^{\mathrm{T}}$. The *type IV singularity* set is defined as

$$S^{(4)} \equiv \{\mathbf{p} = [\hat{\mathbf{p}} \cup \partial\mathbf{q}(\mathbf{t}^{\text{limit}} \text{ or } \mathbf{t}^{\text{inst}})] : \mathrm{Rank}[\boldsymbol{\Phi}_{\mathbf{q}}(\mathbf{w}, \partial\mathbf{q}(\mathbf{t}^{\text{limit}} \text{ or } \mathbf{t}^{\text{inst}}))] < 3, \quad \text{for some } \hat{\mathbf{p}} \in \mathbf{w}, \ \mathbf{dim}(\partial\mathbf{q}(\mathbf{t}^{\text{limit}} \text{ or } \mathbf{t}^{\text{inst}})) \leqslant (n-3)\}. \tag{18}$$

The singular set for the manipulator is a combination of the above four types of singularity sets: $S^{(1)}$, $S^{(2)}$, $S^{(3)}$, and $S^{(4)}$, such that

$$S = S^{(1)} \cup S^{(2)} \cup S^{(3)} \cup S^{(4)} = \{\mathbf{p}^1, \mathbf{p}^2, \ldots, \mathbf{p}^{ns}\}, \tag{19}$$

where ns is the total number of singular vectors $\mathbf{p}$. Substituting these singular vectors into the position vector function of the end-effector in Eq. (1) yields ns parametric singular entities

$$\boldsymbol{\chi}^i(\mathbf{u}^i|\mathbf{p}^i) \quad \text{for } i = 1, \ldots, ns. \tag{20}$$

In general, unless otherwise stated, those entities are parametric surfaces and are denoted by *singular surfaces*. The vector $\mathbf{u}^i$ represents the joint coordinates used as the parameters of the singular surface i, and $\mathbf{p}^i$ is the constant singular vector.

2.3. Determining the boundary

In order to determine the intersection between two parametric surfaces, one parameterized as

$$\boldsymbol{\chi}^1(u, v), \quad u_1 \leqslant u \leqslant u_2, \quad v_1 \leqslant v \leqslant v_2 \tag{21}$$

and the other parameterized as

$$\boldsymbol{\chi}^2(s, w), \quad s_1 \leqslant s \leqslant s_2, \quad w_1 \leqslant w \leqslant w_2, \tag{22}$$

a solution to the following equation is necessary:

$$\boldsymbol{\chi}^1(u, v) - \boldsymbol{\chi}^2(s, w) = \mathbf{0} \tag{23}$$

subject to inequality constraints imposed on the joints in the form of Eq. (6). Eq. (23) can thus be augmented by the inequality constraints as

$$\mathbf{G}(\boldsymbol{\mu}) = \begin{bmatrix} \boldsymbol{\chi}^1(u, v) - \boldsymbol{\chi}^2(s, w) \\ u - \dfrac{u_1 + u_2}{2} - \dfrac{(u_2 - u_1)}{2}\sin\ \kappa_1 \\ v - \dfrac{v_1 + v_2}{2} - \dfrac{(v_2 - v_1)}{2}\sin\ \kappa_2 \\ s - \dfrac{s_1 + s_2}{2} - \dfrac{(s_2 - s_1)}{2}\sin\ \kappa_3 \\ w - \dfrac{w_1 + w_2}{2} - \dfrac{(w_2 - w_1)}{2}\sin\ \kappa_4 \end{bmatrix}, \tag{24}$$

where $\boldsymbol{\mu} = \begin{bmatrix} u & v & s & w & \kappa_1 & \kappa_2 & \kappa_3 & \kappa_4 \end{bmatrix}^{\mathrm{T}}$. Since the Jacobian of $\mathbf{G}(\boldsymbol{\mu})$ is not square, the problem of obtaining an initial solution (initial point) can be solved using the Moore–Penrose inverse [5]. The new generalized coordinates are calculated by evaluating

$$\Delta\boldsymbol{\mu} = \mathbf{G}_{\boldsymbol{\mu}}^{*}(-\mathbf{G}), \tag{25}$$

where $\mathbf{G}_{\boldsymbol{\mu}}^{*}$ is the Moore–Penrose pseudoinverse of the Jacobian $\mathbf{G}_{\boldsymbol{\mu}} = [\partial G_i/\partial\mu_i]$, defined by

$$\mathbf{G}_{\boldsymbol{\mu}}^{*} = \mathbf{G}_{\boldsymbol{\mu}}^{\mathrm{T}}(\mathbf{G}_{\boldsymbol{\mu}}\mathbf{G}_{\boldsymbol{\mu}}^{\mathrm{T}})^{-1}. \tag{26}$$

This method converges within a few iterations without adding any new constraints [5]. Another method for determining a starting point for a surface–surface intersection problem was developed by Muellenheim [25]. Once a starting point is found, the intersection curve is traced along the tangent direction by using the so-called marching method developed by Pratt and Geisow [26]. The algorithm requires a vector tangent direction to compute marching parameters. Let $\boldsymbol{\chi}_u^1$ denote the derivative of $\boldsymbol{\chi}^1$ with respect to u and $\boldsymbol{\chi}_v^1$ denote the derivative of $\boldsymbol{\chi}^1$ with respect to v. The cross-product of these vectors

results in a normal vector to the surface such that

$$\mathbf{N}^1 = (\boldsymbol{\chi}_u^1 \times \boldsymbol{\chi}_v^1)/||\boldsymbol{\chi}_u^1 \times \boldsymbol{\chi}_v^1||. \tag{27}$$

Similarly, the normal vector at a point on the second surface is defined by

$$\mathbf{N}^2 = (\boldsymbol{\chi}_s^2 \times \boldsymbol{\chi}_w^2)/||\boldsymbol{\chi}_s^2 \times \boldsymbol{\chi}_w^2||. \tag{28}$$

The tangent vector $\boldsymbol{\tau}$ is computed as

$$\boldsymbol{\tau} = \mathbf{N}^1 \times \mathbf{N}^2. \tag{29}$$

The new step constraint equation can be written as

$$[\boldsymbol{\chi}^1(u, v) - \boldsymbol{\chi}^0] \cdot \boldsymbol{\tau} - c = 0, \tag{30}$$

where $\boldsymbol{\chi}^0$ is the computed point, and c is the step size.

Although this method will converge to a solution, it is possible to find only one starting point, and thus only one corresponding branch of intersection will be traced. The problem of numerically determining the intersection curve is complicated when several curves exist, in which case tangents at the bifurcation point have to be computed.

The physical significance of singular curves stems from having two constant generalized coordinates, i.e., the manipulator loses at least two degrees of mobility. These singular curves partition singular surfaces into a number of regions called subsurfaces denoted by $\boldsymbol{\psi}^i$. For a singular surface, the intersection of curves c^k results in nodes $\mathbf{N}^j$. For example, to determine subsurfaces on surface $\boldsymbol{\chi}^3$ in Fig. 2(a), it is intersected with $\boldsymbol{\chi}^2$ and $\boldsymbol{\chi}^1$ as depicted in Fig. 2(b). The curves partition this surface to four subsurfaces each bounded by curve segments. These intersections were found by using a rectangular grid as shown in Fig. 2(c). Two curves are checked to see whether they exist inside an incremental rectangle. The tolerance (rectangle width) is subsequently decreased. Difficulties in computing the intersection of singular curves may arise if the curves are interesting at more than one point (along the segment).

Subsurfaces resulting from internal, boundary, and higher-order singularities are computed. Determining whether these subsurfaces are internal or boundary surfaces remains. This can be performed by perturbing a known point on the subsurface and determining whether the perturbed points satisfy the constraint equation. Any point can be chosen, provided that it is not on the boundary of the subsurface. For subsurface $\boldsymbol{\psi}^i(u_1, v_1)$, the partial derivatives with respect to the parameterization variables u_1 and v_1 are $\partial\boldsymbol{\psi}^i/\partial u_1$ and $\partial\boldsymbol{\psi}^i/\partial v_1$. At any regular point $\hat{\mathbf{u}}^o$ on the subsurface, these vectors are linearly independent and tangent to the coordinate curves through $\hat{\mathbf{u}}^o$. The unit vector is

$$\mathbf{n}^0 = \left(\frac{\partial\boldsymbol{\psi}^i}{\partial u_1} \times \frac{\partial\boldsymbol{\psi}^i}{\partial v_1}\right) \Big/ \left\|\frac{\partial\boldsymbol{\psi}^i}{\partial u_1} \times \frac{\partial\boldsymbol{\psi}^i}{\partial v_1}\right\|. \tag{31}$$

For a small perturbation $\partial\varepsilon$ about this point and along the normal vector $\mathbf{n}^0$, the coordinates of the perturbed point can be calculated as

$$\mathbf{x}^p = \boldsymbol{\psi}^i(\hat{\mathbf{u}}^o) \pm \partial\varepsilon\mathbf{n}^0. \tag{32}$$

For the perturbed point to exist within the workspace, it has to satisfy the constraint equation (7), such that a solution to the following equation exists:

$$\begin{bmatrix} \mathbf{x}^p - \boldsymbol{\Phi}(\mathbf{q}(\mathbf{t})) \\ \mathbf{q}(\mathbf{t}) - \mathbf{q}(\mathbf{t}^0) \\ \mathbf{t} - \boldsymbol{\Pi}(\boldsymbol{\lambda}) \end{bmatrix} = \mathbf{0}. \tag{33}$$

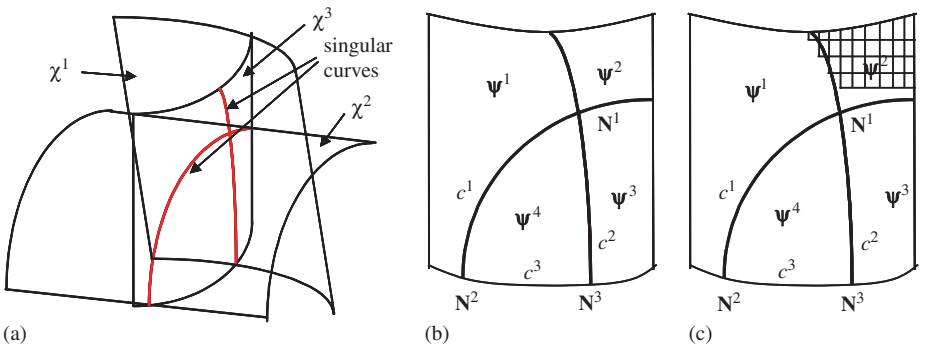

Fig. 2. The intersection and partition of singular surfaces.

The subsurface ψ^i is an internal surface if and only if there exist solutions of Eq. (33) for both perturbations of $\pm\partial\varepsilon$. Otherwise, it will be on the boundary of the workspace.

3. Illustrative examples

In this section, two examples are provided to demonstrate the formulation for determining the workspace boundaries of the manipulators with non-unilateral constraints, and to visualize their workspace. The first one is a 3-DOF spatial example; the second, a 4-DOF spatial example.

3.1. 3-DOF RRR example

A 3-DOF spatial manipulator in Fig. 3 is an example showing the formulation for determining the workspace of this manipulator. DH parameters are shown in Table 1.

The joint profiles are defined as $q_1(t_1) = -2.26893t_1^2 + 6.80678t_1 - \pi/4$, $q_2(t_2) = 1.5708t_2 - \pi/4$, $q_3(t_3) = \pi t_3$, where $0 \leqslant t_1 \leqslant 1.91602$, $0 \leqslant t_2 \leqslant 1.5$, $0 \leqslant t_3 \leqslant 2.0$.

The position vector of the end-effector is formulated as

$$\mathbf{\Phi}(\mathbf{q}(\mathbf{t})) = \begin{bmatrix} 10\cos q_1\cos q_2\cos q_3 - 10\sin q_1\sin q_3 - 10\cos q_1\sin q_2 + 20\cos q_1\cos q_2 \\ 10\sin q_1\cos q_2\cos q_3 + 10\cos q_1\sin q_3 - 10\sin q_1\sin q_2 + 20\sin q_1\cos q_2 \\ 10\sin q_2\cos q_3 + 10\cos q_2 + 20\sin q_2 + 50 \end{bmatrix} \tag{34}$$

and the inequality constraints are parameterized as $t_1 = 0.95801 + 0.95801\sin\lambda_1$, $t_2 = 0.75 + 0.75\sin\lambda_2$, $t_3 = 1 + \sin\lambda_3$, where $\mathbf{t} = [\,t_1 \quad t_2 \quad t_3\,]^{\mathrm{T}}$, $\boldsymbol{\lambda} = [\,\lambda_1 \quad \lambda_2 \quad \lambda_3\,]^{\mathrm{T}}$.

The Jacobian matrix is derived as

$$[\mathbf{H}_{\mathbf{q}^*}] = \begin{bmatrix} \mathbf{\Phi}_{\mathbf{q}} & \mathbf{0}_1 & \mathbf{0}_2 \\ \mathbf{I} & \mathbf{\Gamma}_{\mathbf{t}} & \mathbf{0}_3 \\ \mathbf{0}_4 & \mathbf{I} & \mathbf{t}_{\boldsymbol{\lambda}} \end{bmatrix}_{9\times 9}, \tag{35}$$

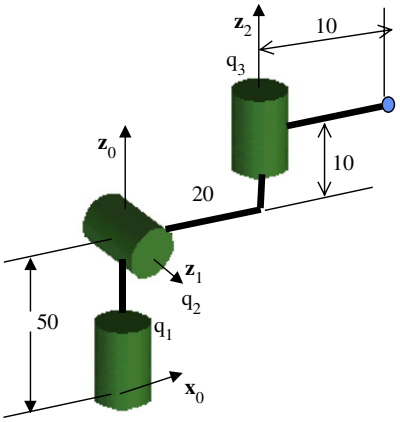

Fig. 3. A spatial 3-DOF RRR manipulator.

Table 1
DH table for the spatial 3-DOF RRR manipulator

	θ_i	d_i	a_i	α_i
1	q_1	50	0	$\pi/2$
2	q_2	0	20	$-\pi/2$
3	q_3	10	10	0

where

$$\mathbf{\Phi_q} = \begin{bmatrix} -10(c_2(2+c_3)s_1 - s_1s_2 + c_1s_3) & -10(c_1(c_2+(2+c_3)s_2) & -10(c_3s_1 + c_1c_2s_3) \\ 10(c_1(c_2(2+c_3) - s_2) & -10s_1(c_2+(2+c_3)s_2) & 10(c_1c_3 - c_2s_1s_3) \\ 0 & 10(c_2(2+c_3) - s_2) & -10s_2s_3 \end{bmatrix},$$

$$\mathbf{\Gamma_t} = \begin{bmatrix} 6.80678 - 4.53786t_1 & 0 & 0 \\ 0 & 1.5708 & 0 \\ 0 & 0 & \pi \end{bmatrix},$$

$$\mathbf{t_\lambda} = \begin{bmatrix} -0.95801\cos\lambda_1 & 0 & 0 \\ 0 & -0.75\cos\lambda_2 & 0 \\ 0 & 0 & -\cos\lambda_3 \end{bmatrix}.$$

3.1.1. Type I: Jacobian singularities

Since $[\mathbf{\Phi_q}]$ is a (3×3) block matrix, there is only one equation that is equal to zero.

$$Det[\mathbf{\Phi_q}] = -2000(\cos q_2(2+\cos q_3) - \sin q_2)\sin q_3 = 0. \tag{36}$$

Solving Eq. (36) yields $q_3 = 0$ or $q_3 = \pi$ Therefore, Jacobian singular sets are $\mathbf{p}_1 = \{q_3(0)\}$, $\mathbf{p}_2 = \{q_3(1)\}$.

3.2. Type II: instantaneous singularities

$\mathbf{\Gamma_t}$ is a (3×3) matrix, and applying the rank deficiency condition to $\mathbf{\Gamma_t}$ yields

$$Det[\mathbf{\Gamma_t}] = 1.5708\pi(6.80678 - 4.53786t_1) = 0. \tag{37}$$

The singular set is therefore $\mathbf{p}_3 = \{q_1(1.5)\}$.

3.2.1. Type III singularities

Type III singular sets include $\mathbf{p}_4 = \{q_1(0)\}$, $\mathbf{p}_5 = \{q_1(1.91602)\}$, $\mathbf{p}_6 = \{q_2(0)\}$, $\mathbf{p}_7 = \{q_2(2.0)\}$.

There is no Type IV singularity set because this is a 3-DOF problem. The singular surfaces are shown in Fig. 4.

3.3. Determining subsurfaces

Singular surfaces are divided into subsurfaces by computing curves of intersection between them. Once these curves are determined and projected onto their respective parametric space of two variables, each region representing a subsurface is studied for existence on the boundary of the workspace. To illustrate the determination of subsurfaces, consider the intersection of the two surfaces χ_4 and χ_5. The marching method presented in previous section is implemented. The constraint matrix (Eq. (24)) can be written as

$$\mathbf{G}(\boldsymbol{\mu}) = \begin{bmatrix} \chi^1(u,v) - \chi^2(s,w) \\ u - \pi - \pi\sin\kappa_1 \\ v - \frac{\pi}{8} - \frac{3\pi}{8}\sin\kappa_2 \\ s - \pi - \pi\sin\kappa_3 \\ w - \frac{\pi}{8} - \frac{3\pi}{8}\sin\kappa_4 \end{bmatrix}. \tag{38}$$

The starting point $\boldsymbol{\mu}^*$ computed using the Moore–Penrose pseudo inverse is $\boldsymbol{\mu}^* = [0.6184 \quad 3.4086 \quad 0.6184 \quad 2.8745 \quad 0.1928 \quad 0.0851 \quad 0.1928 \quad -0.0851]$. Using $\boldsymbol{\mu}^*$ as a starting point, the algorithm for mapping marching curves is employed to continue tracing the curves. In this special case, a bifurcation point is encountered at $\boldsymbol{\mu}^o = [0.7854 \quad 3.1416 \quad 0.7854 \quad 3.1416 \quad 0.3398 \quad 0.8306\times 10^{-9} \quad 0.3398 \quad -0.8306\times 10^{-9}]$. Two tangents are required to continue tracing. The computed intersection curves in the parametric space are depicted in Fig. 5(a), and depicted on the surfaces in Fig. 5(b).

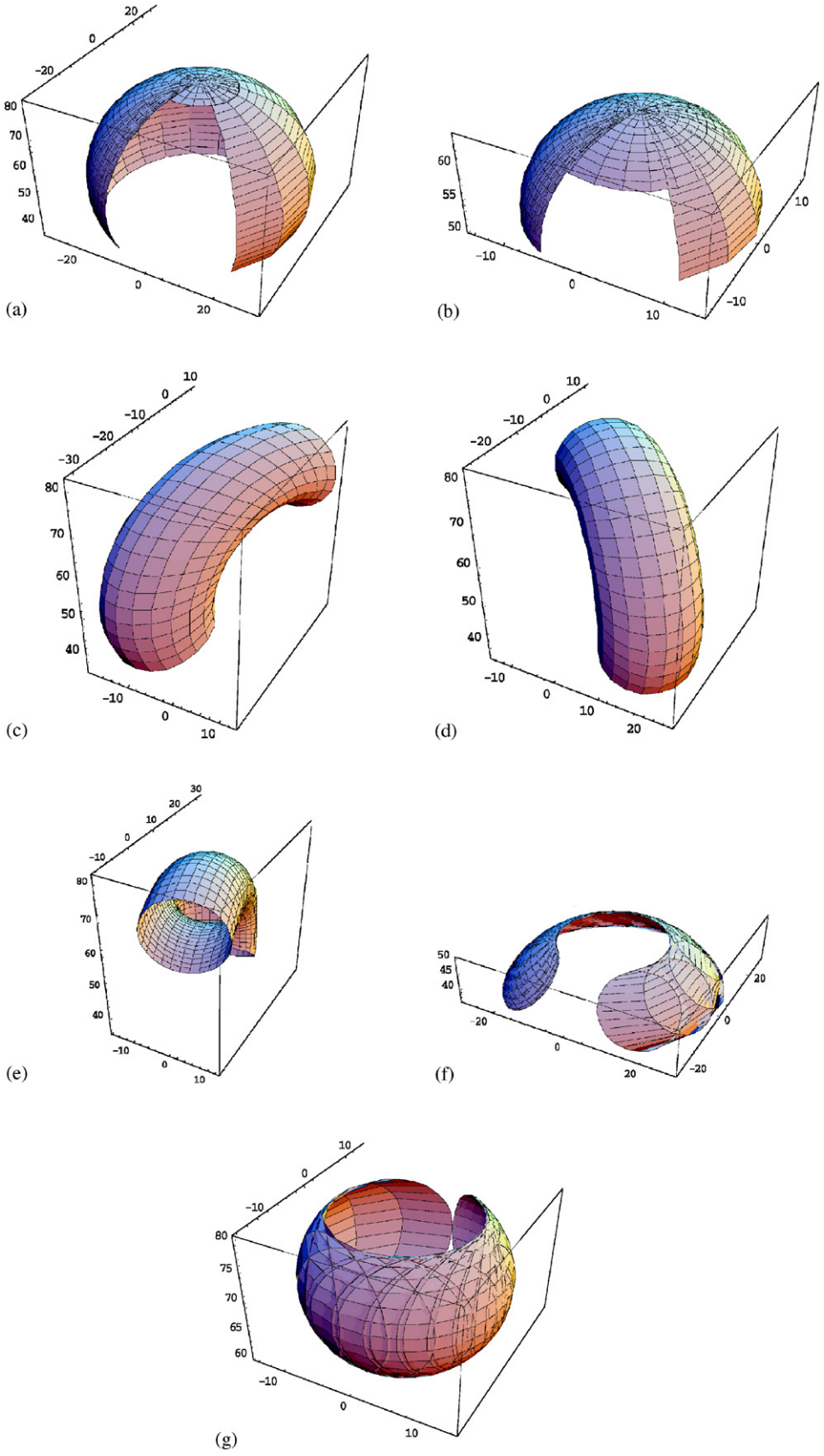

Fig. 4. Singular surfaces: (a) singular surface $\chi_{1;}$ (b) singular surface χ_2; (c) singular surface χ_3; (d) singular surface χ_4; (e) singular surface χ_5; (f) singular surface χ_6; and (g) singular surface χ_7.

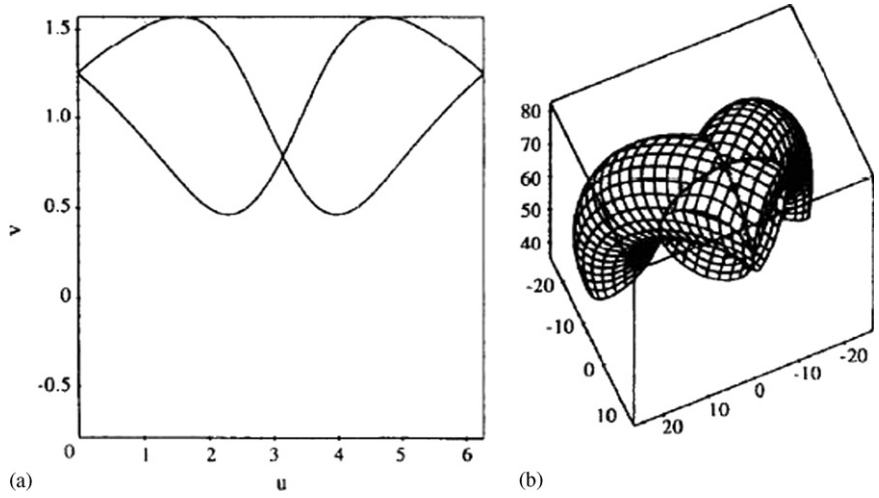

Fig. 5. Intersection curves between χ_4 and χ_5; (a) In the *uv* space; (b) on the surfaces.

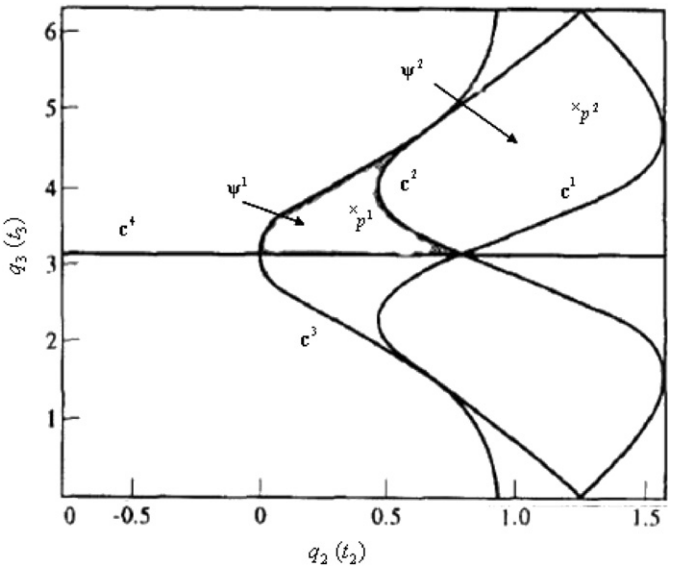

Fig. 6. Singular surface χ_4 is divided into several subsurfaces.

In addition to the intersection curves resulting from the intersection between χ_4 and χ_5, surface χ_4 intersects with other singular surfaces. The computed intersection curves due to other singular surfaces are superpositioned in Fig. 6. These four singular curves (c^1, c^2, c^3 and c^4) partition surface χ_4 into 12 subsurfaces.

It is necessary to determine the intersection of these curves in order to define the boundary of each subsurface. Singular curves shown in Fig. 7 are computed numerically, thus, it is difficult to parameterize these curves. The grid method is thus used to determine points of intersection.

To determine whether each subsurface is a boundary or internal subsurface to the wrist workspace, the perturbation method is implemented. For example, consider the point p^1 on the subsurface ψ^1 which has the set of generalized coordinates $q_2(0.754646) = 0.4$ and $q_3(1.08225) = 3.4$. Note that the subsurface ψ^1 is defined as follows:

$$\psi^1 = \begin{bmatrix} 7.0711\cos q_2\cos q_3 + 7.0711(\sin q_3 - \sin q_2) + 14.1421\cos q_2 \\ -7.0711\cos q_2\cos q_3 + 7.0711(\sin q_3 + \sin q_3) - 14.1421\cos q_2 \\ 10\cos q_2\sin q_3 + 10\cos q_2 + 20\sin q_2 + 50 \end{bmatrix} \tag{39}$$

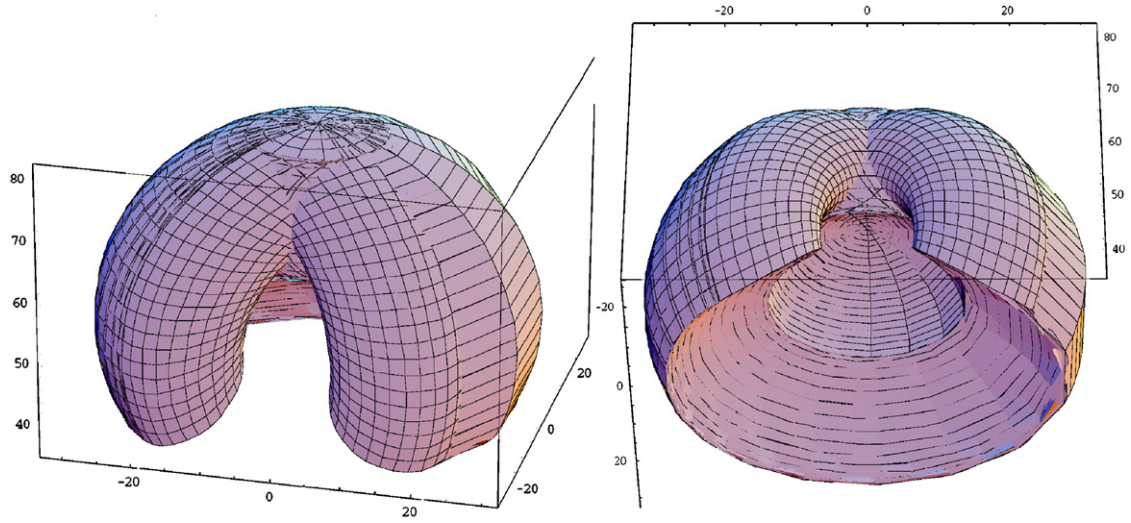

Fig. 7. Two views of the enveloped workspace for spatial RRR manipulator.

and it is shown in Fig. 7. To determine the normal to $\boldsymbol{\psi}^1$ using Eq. (39), partial derivatives representing tangent vectors are evaluated such that

$$\frac{\partial \boldsymbol{\psi}^1}{\partial q_2} = \begin{bmatrix} -7.07 \sin q_2 \cos q_3 - 7.07 \cos q_2 - 14.14 \sin q_2 \\ 7.07 \sin q_2 \cos q_3 + 7.07 \cos q_2 + 14.14 \sin q_2 \\ 10 \cos q_2 \cos q_3 - 10 \sin q_2 + 20 \cos q_2 \end{bmatrix} \tag{40}$$

and

$$\frac{\partial \boldsymbol{\psi}^1}{\partial q_3} = \begin{bmatrix} -7.07 \cos q_2 \sin q_3 + 7.07 \cos q_3 \\ 7.07 \cos q_2 \sin q_3 + 7.07 \cos q_3 \\ -10 \sin q_2 \sin q_3 \end{bmatrix}. \tag{41}$$

The normal is computed

$$\mathbf{n} = \frac{\partial \psi^1}{\partial q_2} \times \frac{\partial \psi^1}{\partial q_3} = \begin{bmatrix} \frac{707}{-10}(\cos q_2 (\cos q_3)^2 - \sin q_3 \cos q_3 - \sin q_3 + \sin q_2 \cos q_3 - 2 \cos q_2 \cos q_3) \\ \frac{707}{-10}(\cos q_3 \sin q_2 + \cos q_2 (\cos q_3)^2 - 2 \sin q_3 - \cos q_3 \sin q_3 + \cos q_2 \cos q_3) \\ \frac{499849}{-5000}(\sin q_2 \cos q_3 - \cos q_2 \cos q_3 - \sin q_2 (\cos q_3)^2) \end{bmatrix}. \tag{42}$$

The unit normal $\mathbf{n}^0 = \mathbf{n}/||\mathbf{n}||$ at the point $\hat{\mathbf{u}}^o$ on the subsurface $\boldsymbol{\psi}^1$ is evaluated

$$\mathbf{n}^0 = \left(\frac{\partial \boldsymbol{\psi}^1}{\partial q_2} \times \frac{\partial \boldsymbol{\psi}^1}{\partial q_3}\right) \Big/ \left\| \frac{\partial \boldsymbol{\psi}^1}{\partial q_2} \times \frac{\partial \boldsymbol{\psi}^1}{\partial q_3} \right\| = [0.098 \quad -0.452 \quad 0.887]^{\mathrm{T}}.$$

For a small perturbation $\partial\varepsilon = +0.1$, the coordinates of the perturbed point are computed as

$$\mathbf{x}^{p^+} = \boldsymbol{\psi}^1(\mathbf{z}^0) + 0.1\mathbf{n}^0 = [6.513 \quad -1.812 \quad 63.418]^{\mathrm{T}}.$$

Solving Eq. (33) by the modified Newton–Raphson method, the iterations converge to a solution $\mathbf{z} = [2.321 \quad 1.222 \quad -3.502]^{\mathrm{T}}$. Similarly, the other perturbed point $\mathbf{x}^{p^-}$ due to $\partial\varepsilon = -0.1$ can be computed as

$$\mathbf{x}^{p^-} = \boldsymbol{\psi}^1(\mathbf{z}^0) - 0.1\mathbf{n}^0 = [6.494 \quad -1.721 \quad 63.241]^{\mathrm{T}}.$$

The iterations also converge to a solution $\mathbf{z} = [2.393 \quad 1.231 \quad -3.463]^{\mathrm{T}}$. Thus, both perturbation points are inside the workspace. Therefore, the subsurface $\boldsymbol{\psi}^1$ is an internal subsurface. For example, select the point p^2 on the subsurface $\boldsymbol{\psi}^2$, which has joint coordinates $\mathbf{z}^0 = [q_2(1.13662) \quad q_3(1.40056) \quad q_1(0)]^{\mathrm{T}}$. The normal vector at this point is calculated as

$$\mathbf{n}^0 = [0.098 \quad -0.452 \quad 0.887]^{\mathrm{T}}.$$

For a small positive perturbation $\partial\varepsilon = +0.1$, the perturbed point is

$$\mathbf{x}^{p^+} = [-6.211 \quad -7.245 \quad 69.646]^{\mathrm{T}}.$$

Solving the corresponding equation of Eq. (29), a convergence solution can be obtained as $\mathbf{z} = [2.276 \quad 1.114 \quad 1.882]^{\mathrm{T}}$. However, a solution cannot be found for the negative perturbation point with $\partial\varepsilon = -0.1$. This indicates that $\boldsymbol{\psi}^2$ is a boundary subsurface of the workspace.

Using this technique, the boundary subsurfaces of each singular surface are identified. These surfaces are depicted in Fig. 7, from two different points of views. The volume enclosed by these surfaces is the workspace.

3.4. 4-DOF RPRP example

A spatial 4-DOF manipulator is shown in Fig. 8. The manipulator has 2 revolute and 2 prismatic joints and its DH parameters are presented in Table 2.

The joint profiles are defined as $q_1(t_1) = \pi t_1$, $q_2(t_2) = 12t_2 + 20$, $q_3(t_3) = -7\pi/4t_3^2 + 3.5\pi t_3 - \pi/4$, $q_4(t_4) = -6.667t_4^2 + 20t_4 + 10$, where $0 \leqslant t_1 \leqslant 2$, $0 \leqslant t_2 \leqslant 2.5$, $0 \leqslant t_3 \leqslant 1.53452$, $0 \leqslant t_4 \leqslant 2.36586$.

The position vector of the end-effector is formulated as

$$\mathbf{x} = \boldsymbol{\Phi}(\mathbf{q}(\mathbf{t})) = \begin{bmatrix} q_4 \cos q_1 \cos q_3 + 30 \cos q_1 \\ q_4 \sin q_1 \cos q_3 + 30 \sin q_1 \\ q_4 \sin q_3 + q_2 \end{bmatrix} \tag{43}$$

and the inequality constraints are parameterized as $t_1 = 1 + \sin \lambda_1$, $t_2 = 1.25 + 1.25 \sin \lambda_2$, $t_3 = 0.76726 + 0.76726 \sin \lambda_3$, and $t_4 = 1.18293 + 1.18293 \sin \lambda_4$, where $\mathbf{t} = [t_1 \quad t_2 \quad t_3 \quad t_4]^{\mathrm{T}}$, $\boldsymbol{\lambda} = [\lambda_1 \quad \lambda_2 \quad \lambda_3 \quad \lambda_4]^{\mathrm{T}}$.

The Jacobian matrix is derived as

$$[\mathbf{H}_{q^*}] = \begin{bmatrix} \boldsymbol{\Phi}_{\mathbf{q}} & \mathbf{0}_1 & \mathbf{0}_2 \\ \mathbf{I} & \boldsymbol{\Gamma}_{\mathbf{t}} & \mathbf{0}_3 \\ \mathbf{0}_4 & \mathbf{I} & \mathbf{t}_{\boldsymbol{\lambda}} \end{bmatrix}_{11\times 12}, \tag{44}$$

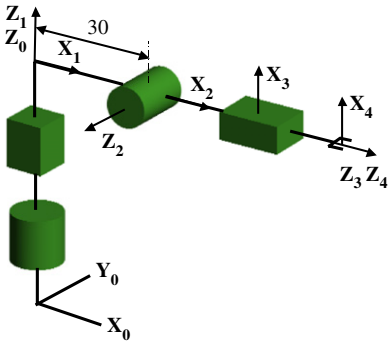

Fig. 8. A spatial 4-DOF RPRP manipulator.

Table 2
DH table for the spatial 4-DOF RPRP manipulator

	θ_i	d_i	α_i	a_i
1	q_1	0	0	0
2	0	q_2	$\pi/2$	30
3	$\pi/2+q_3$	0	$\pi/2$	0
4	0	q_4		

where

$$\mathbf{\Phi_q}(\mathbf{q}) = \begin{bmatrix} -q_4 \sin q_1 \cos q_3 - 30 \sin q_1 & 0 & -q_4 \cos q_1 \sin q_3 & \cos q_1 \cos q_3 \\ q_4 \cos q_1 \cos q_3 + 30 \cos q_1 & 0 & -q_4 \sin q_1 \sin q_3 & \sin q_1 \cos q_3 \\ 0 & 1 & q_4 \cos q_3 & \sin q_3 \end{bmatrix}_{3\times 4}, \tag{45}$$

$$\mathbf{\Gamma_t} = \begin{bmatrix} -\pi & 0 & 0 & 0 \\ 0 & -12 & 0 & 0 \\ 0 & 0 & 3.5\pi(t_3 - 1) & 0 \\ 0 & 0 & 0 & 13.334t_4 - 20 \end{bmatrix}_{4\times 4}, \tag{46}$$

$$\mathbf{t_\lambda} = \begin{bmatrix} -\cos\lambda_1 & 0 & 0 & 0 \\ 0 & -1.25\cos\lambda_2 & 0 & 0 \\ 0 & 0 & -0.76726\cos\lambda_3 & 0 \\ 0 & 0 & 0 & -1.18293\cos\lambda_4 \end{bmatrix}_{4\times 4}. \tag{47}$$

3.4.1. Type I: Jacobian singularities

Since $[\mathbf{\Phi_q}]$ is a (3×4) block matrix, there are four equations that are equal to zero and that are to be solved simultaneously. Solution to the simultaneous equations is given by $q_4 = -30\,\mathrm{s}\,q_3$; this solution does not satisfy the joint profiles. Therefore, the rank-deficiency criterion of the Jacobian yields no singular set.

3.5. Type II: instantaneous singularities

Applying the row-rank deficiency condition to Eq. (46), i.e., $Det[\mathbf{\Gamma_t}] = 0$, yields $t_3 = 1.0$, and $t_4 = 1.5$. Therefore, an instantaneous singularity set is identified as $\mathbf{p}_1 = \{q_3(1.0), q_4(1.5)\}$.

3.5.1. Type III singularities

This includes combinations of joint outer limits and instantaneous limits as follows: $\mathbf{p}_2 = \{q_3(1.53452), q_4(0)\}$, $\mathbf{p}_3 = \{q_3(1.53452), q_4(2.36586)\}$, $\mathbf{p}_4 = \{q_2(0), q_3(0)\}$, $\mathbf{p}_5 = \{q_2(0), q_3(1.53452)\}$, $\mathbf{p}_6 = \{q_2(0), q_4(0)\}$, $\mathbf{p}_7 = \{q_2(0), q_4(2.36586)\}$, $\mathbf{p}_8 = \{q_2(2.5), q_3(0)\}$, $\mathbf{p}_9 = \{q_2(2.5), q_4(0)\}$, $\mathbf{p}_{10} = \{q_2(2.5), q_4(2.36586)\}$, $\mathbf{p}_{11} = \{q_3(0), q_4(0)\}$, $\mathbf{p}_{12} = \{q_3(0), q_4(2.36586)\}$, $\mathbf{p}_{13} = \{q_3(1), q_4(0)\}$, $\mathbf{p}_{14} = \{q_3(1), q_4(2.36586)\}$, $\mathbf{p}_{15} = \{q_2(0), q_3(1)\}$, $\mathbf{p}_{16} = \{q_2(2.5), q_3(1)\}$, $\mathbf{p}_{17} = \{q_1(0), q_3(1)\}$, $\mathbf{p}_{18} = \{q_1(2), q_3(1)\}$, $\mathbf{p}_{19} = \{q_3(0), q_4(1.5)\}$, $\mathbf{p}_{20} = \{q_3(1.53452), q_4(1.5)\}$, $\mathbf{p}_{21} = \{q_2(0), q_4(1.5)\}$, $\mathbf{p}_{22} = \{q_2(2.5), q_4(1.5)\}$, $\mathbf{p}_{23} = \{q_1(0), q_4(1.5)\}$, $\mathbf{p}_{24} = \{q_1(2.5), q_4(1.5)\}$.

3.5.2. Type IV: coupled singularities

The block $\mathbf{t_\lambda}$ is rank deficient at $t_4 = 0$. Substituting $t_4 = 0$ into $\mathbf{\Phi(q)}$, computing $[\mathbf{\Phi_q}]$, then $[\mathbf{\Phi_q} \not\subset \mathbf{\Phi}_{q_4}]$ is defined as

$$[\mathbf{\Phi_q} \not\subset \mathbf{\Phi}_{q_4}] = \begin{bmatrix} -30 \sin q_1 - 10 \cos q_3 \sin q_1 & 0 & -10 \cos q_1 \sin q_3 \\ -30 \cos q_1 + 10 \cos q_3 \cos q_1 & 0 & -10 \sin q_1 \sin q_3 \\ 0 & 1 & 10 \cos q_3 \end{bmatrix}$$

and applying the rank deficiency condition to $[\mathbf{\Phi_q} \not\subset \mathbf{\Phi}_{q_4}]$, where $\partial\mathbf{q}(\mathbf{t}^{\mathrm{limit}}) = q_4(t_4^{\mathrm{L}})$, yields a solution $q_3 = 0$, which is at $t_3 = 0.07418$. Therefore, a singular set is identified as $\mathbf{p} = [\hat{\mathbf{p}}, \partial\mathbf{q}(\mathbf{t}^{\mathrm{limit}})] = \mathbf{p}_{25} = \{q_3(0.07418), q_4(0)\}$, similarly, $\mathbf{p}_{26} = \{q_3(0.07418), q_4(2.36586)\}$.

The block $\mathbf{\Gamma_t}$ is rank deficient at $t_4 = 1.5$. Substituting $t_4 = 1.5$ into $\mathbf{\Phi(q)}$, computing $[\mathbf{\Phi_q}]$, then $[\mathbf{\Phi_q} \not\subset \mathbf{\Phi}_{q_4}]$ is defined

$$JJ = \begin{bmatrix} -30 \sin q_1 - 25 \cos q_3 \sin q_1 & 0 & -25 \cos q_1 \sin q_3 \\ -30 \cos q_1 + 25 \cos q_3 \cos q_1 & 0 & -25 \sin q_1 \sin q_3 \\ 0 & 1 & 25 \cos q_3 \end{bmatrix},$$

and applying the rank deficiency condition to JJ where $\partial\mathbf{q}(\mathbf{t}^{\mathrm{inst}}) = q_4(t_4^{\mathrm{inst}})$ yields a solution $q_3 = 0$, which is at $t_3 = 0.07418$. Therefore a singular set is identified as $\mathbf{p}_{27} = \{q_3(0.07418), q_4(1.5)\}$. Substituting each singularity set into Eqs. (43) yields parametric equations of singular surfaces in $\mathbf{R}^3$. Fig. 9 shows the cross sections of singular surfaces due to different singular sets.

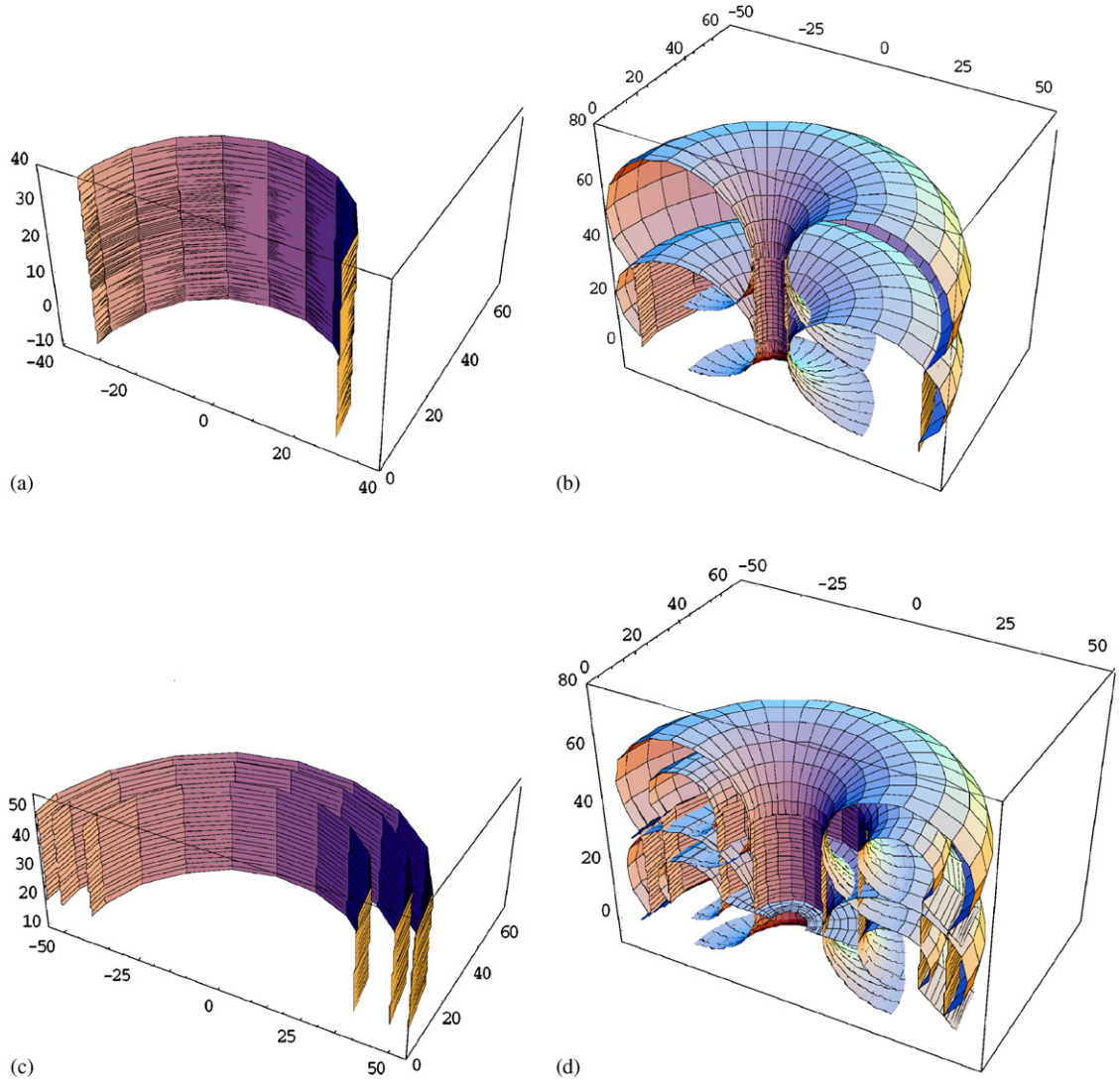

Fig. 9. Cross–sections of the singular surfaces: (a) due to $\mathbf{p}_1$ and $\mathbf{p}_{13},\ldots,\mathbf{p}_{18}$; (b) due to $\mathbf{p}_{19},\ldots,\mathbf{p}_{21}$; (c) due to $\mathbf{p}_{25}$, $\mathbf{p}_{26}$, $\mathbf{p}_{27}$; and (d) due to $\mathbf{p}_2,\ldots,\mathbf{p}_{12}$.

Applying the surface intersection method and the boundary identification algorithm presented in Section 2 yields the final enveloped workspace of the 4-DOF RPRP manipulator shown in Fig. 10.

4. Conclusions

A general formulation for determining workspace boundaries in closed form for general serial manipulators with non-unilateral constraints has been presented. The workspace constraint function was formulated in terms of generalized coordinates, including inequality constraints imposed on each joint's time function. It was shown that Jacobian row-rank deficiency conditions used to determine degenerate conditions can be employed here to generate constant singular sets and to identify coupled singular behavior, where four distinct types of singular sets have been identified. It was shown that the formulation can be characterized as a constraint function, whose Jacobian rank deficiency provides a rigorous, consistent method for delineating singular behavior. It was also shown that by using a surface-surface intersection method the singular surfaces will be divided into subsurfaces. A general visualization algorithm (perturbation method) can then be implemented to depict the boundary subsurfaces of the workspace envelope. From this study it was shown that although there are more singular surfaces for non-unilateral constraints compared to unilateral constraints, for the same serial manipulator and same range of motions, the final workspace boundary is the same for unilateral and non-unilateral constraints.

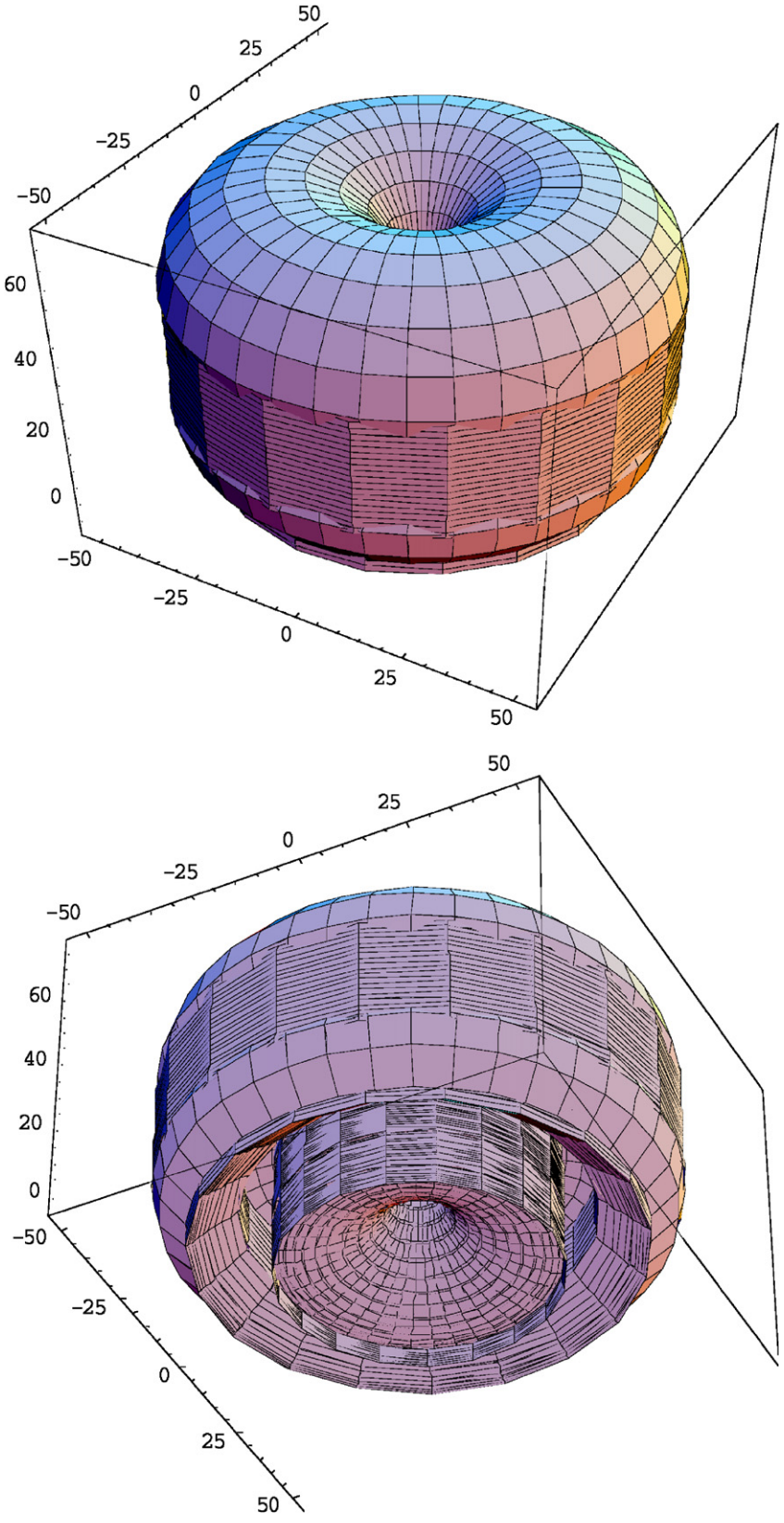

Fig. 10. Two views of the enveloped workspace of a 4-DOF RPRP manipulator.

References

[1] Abdel-Malek K, Yeh HJ. Analytical boundary of the workspace for general 3-DOF mechanisms. Int J Robot Res 1997;16(2):1–12.
[2] Abdel-Malek K, Yeh HJ, Khairallah N. Workspace, void, and volume determination of the general 5DOF manipulator. Mech Struct Mach 1999;27(1):91–117.
[3] Abdel-Malek K, Adkins F, Yeh HJ, Haug EJ. On the determination of boundaries of manipulator workspaces. Robot Comput-Int Manuf 1997;13(1):63–72.
[4] Agrawal SK. Workspace boundaries of in-parallel manipulator systems. Int J Robot Automat 1990;7(2):94–9.
[5] Allgower EL, Geog K. Numerical continuation methods: an introduction. Berlin, Germany: Springer; 1990.
[6] Bulca F, Angeles J, Zsombor-Murray PJ. On the workspace determination of spherical serial and platform mechanisms. Mech Mach Theory 1999;34(3):497–512.
[7] Cavusoqlu MC, Villanueva I, Tendick F. Workspace analysis of robotic manipulators for a teleoperated suturing task. IEEE Int Conf Intell Robot Syst 2001;4:2234–9.
[8] Ceccarelli M, Vinciguerra A. On the workspace of general 4R manipulators. Int J Robot Res 1995;14(2):152–60.
[9] Ceccarelli M. A synthesis algorithm for three-revolute manipulators by using an algebraic formulation of workspace boundary. ASME J Mech Des 1995;117(2(A)):298–302.
[10] Ceccarelli M, Ottaviano E. A workspace evaluation of an eclipse robot. Robotica 2002;20(3):299–313.
[11] Davidson JK, Hunt KH. Rigid body location and robot workspace: some alternative manipulator forms. Issue Series Title: J Mech Transm-T ASME 1987;109(2):224–32.
[12] Denavit J, Hartenberg RS. A kinematic notation for lower-pair mechanisms based on matrices. J Appl Mech, ASME 1955;22:215–21.
[13] Di Gregorio R, Zanforlin R. Workspace analytic determination of two similar translational parallel manipulators. Robotica 2003;21(5):555–66.
[14] Emiris DM. Workspace analysis of realistic elbow and dual-elbow robot. Mech Mach Theory 1993;28(3):375–96.
[15] Freudenstein F, Primrose EJ. On the analysis and synthesis of the workspace of a three-link, turning-pair connected robot arm. J Mech, Transm Automat Des 1984;106:365–70.
[16] Fu S, Gonzalez J, Lee S. Robotics: control, sensing, vision, and intelligence. New York: McGraw-Hill, Inc.; 1987.
[17] Gosselin C, Angeles J. Singularity analysis of closed loop kinematic chains. IEEE Trans Robotic Automat 1990;6(3):281–90.
[18] Gupta KC. On the nature of robot workspace. Int J Rob Res 1986;5(2):112–21.
[19] Haug EJ, Wang JY, Wu JK. Dextrous workspaces of manipulators: I. analytical criteria. In: Haug EJ, editor. Mech Struct Mach 1992; 20(3): 321–361.
[20] Haug EJ, Luh CM, Adkins FA, Wang JY. Numerical algorithms for mapping boundaries of manipulator workspaces. ASME J Mech Des 1996;118:228–34.
[21] Kumar A, Waldron KJ. The workspace of a mechanical manipulator. ASME J Mech Des 1981;103:665–72.
[22] Lipkin H, Pohl E. Enumeration of singular configurations for robotic manipulators. J Mech Transm-T ASME 1991;113:272–9.
[23] Litvin FL. Application of theorem of implicit function system existence for analysis and synthesis of linkages. Mech Mach Theor 1980;15:115–25.
[24] Monsarrat B, Gosselin CM. Singularity analysis of a three-leg six-degree-of-freedom parallel platform mechanism based on Grassmann line geometry. Int J Robotic Res 2001;20(4):312–26.
[25] Muellenheim G. On determining start points for a surface/surface intersection algorithm. Comput Aided Geom Des 1991;8(5):401–8.
[26] Pratt MJ, Geisow AD. Surface/surface intersection problems. In: Gregory JA, editor. The Math Surf. Oxford, UK: Clarendon Press; 1986.
[27] Pennock GR, Kassner DJ. The workspace of a general planar three-degree-of-freedom platform-type manipulator. J Mech Des 1993;115:269–76.
[28] Qiu CC, Luh CM, Haug EJ. Dexterous workspaces of manipulators, Part III: Calculation of continuation curves at bifurcation points. In: Proceedings of the 21st design automation conference, Boston, MA; 1995.
[29] Roth B. Performance evaluation of manipulators from a kinematic viewpoint. NBS Special Publications 1975;459:39–61.
[30] Shamir T. The singularities of redundant robot arms. Int J Robot Res 1990;2(1):113–21.
[31] Spanos J, Kohli D. Workspace analysis of regional structure of manipulators. Issue Series Title: J Mech Transm-T ASME 1985;107:219–25.
[32] St-Onge BM, Gosselin CM. Singularity analysis and representation of the general Gough–Stewart platform. Int J Robot Res 2000;19(3):271–88.
[33] Sugimoto K, Duffy J. Determination of extreme distances of a robot hand. Part 2: robot arms with special geometry. ASME J Mech Des 1982;104:704–12.
[34] Sugimoto K, Duffy J, Hunt KH. Special configurations of spatial mechanisms and robot arms. Mech Mach Theor 1982;117(2):119–32.
[35] Tsai YC, Soni AH. Accessible region and synthesis of robot arm. ASME J Mech Des 1981;103:803–11.
[36] Vinagradov I. Details of kinematics of manipulators with the method of volumes. Mexanika Mashin 1971(27–28):5–16 [in Russian].
[37] Waldron KJ, Wang SL, Bolin SL. A study of the Jacobian matrix of serial manipulators. Issue Series Title: J Mech Transm-T ASME 1985;107:230–8.
[38] Wang SL, Waldron KJ. Study of the singular configurations of serial manipulators. Issue Series Title: J Mech Transm-T ASME 1987;109:14–20.
[39] Wang JY, Wu JK. Dexterous workspaces of manipulators, Part 2: computational methods. Mech Struct Mach 1993;21(4):471–506.
[40] Wang Y, Newman WS, Stoughton RS. Workspace analysis of the ParaDex robot—a novel, closed-chain, kinematically-redundant manipulator. Proc-IEEE Int Conf Robot Automat 2000;3:2392–7.
[41] Zhang SJ, Sanger DJ, Howard D. Workspaces of a walking machine and their graphical representation. Part I: Kinematic workspaces. Robotica 1996;14:71–9.
[42] Yang DCH, Lee TW. On the workspace of mechanical manipulators. Issue Series Title: J Mech Transm-T ASME 1983;105:62–9.
[43] Yang J, Abdel-Malek K. Singularities of manipulators with non-unilateral constraints. Robotica 2005;23(05):543–53.
[44] Yang J, Abdel-Malek K. On the determination of open-loop manipulator singularities subject to unilateral and non-unilateral constraints. Int J Robot Automat 2006;21(3):218–28.
[45] Snyman JA, du Plessis LJ, Duffy J. An optimization approach to the determination of the boundaries of manipulator workspaces. J Mech Des 2000;122(4):447–56.